Inorganic Chemistry

pubs.acs.org/IC Article

Synthesis, Photophysics, and Reverse Saturable Absorption of *trans*-Bis-cyclometalated Iridium(III) Complexes (C^N^C)Ir(R-tpy)$^+$ (tpy = 2,2′:6′,2″-Terpyridine) with Broadband Excited-State Absorption

Bingqing Liu, Mohammed A. Jabed, Svetlana Kilina, and Wenfang Sun*

Cite This: *Inorg. Chem.* 2020, 59, 8532−8542 Read Online

ACCESS | Metrics & More | Article Recommendations | Supporting Information

ABSTRACT: Extending the bandwidth of triplet excited-state absorption in transition-metal complexes is appealing for developing broadband reverse saturable absorbers. Targeting this goal, five bis-terdentate iridium(III) complexes (**Ir1**-**Ir5**) bearing *trans*-bis-cyclometalating (C^N^C) and 4′-R-2,2′:6′,2″-terpyridine (4′-R-tpy) ligands were synthesized. The effects of the structural variation in cyclometalating ligands and substituents at the tpy ligand on the photophysics of these complexes have been systematically explored using spectroscopic methods (i.e., UV−vis absorption, emission, and transient absorption spectroscopy) and time-dependent density functional theory (TDDFT) calculations. All complexes exhibited intensely structured $^1\pi,\pi^*$ absorption bands at <400 nm and broad charge transfer (^{1}CT)/$^1\pi,\pi^*$ transitions at 400−600 nm. Ligand structural variations exerted a very small effect on the energies of the ^{1}CT/$^1\pi,\pi^*$ transitions; however, they had a significant effect on the molar extinction coefficients of these absorption bands. All complexes emitted featureless deep red phosphorescence in solutions at room temperature and gave broadband and strong triplet excited-state absorption ranging from the visible to the near-infrared (NIR) spectral regions, with both originating from the $^3\pi,\pi^*$/^{3}CT states. Although alteration of the ligand structures influenced the emission energies slightly, these changes significantly affected the emission lifetimes and quantum yields, transient absorption spectral features, and the triplet excited-state quantum yields of the complexes. Except for **Ir3**, the other four complexes all manifested reverse saturable absorption (RSA) upon nanosecond laser pulse excitation at 532 nm, with the decreasing trend of RSA following **Ir2** ≈ **Ir4** > **Ir1** > **Ir5** > **Ir3**. The RSA trend corresponded well with the strength of the excited-state and ground-state absorption differences (ΔOD) at 532 nm for these complexes.

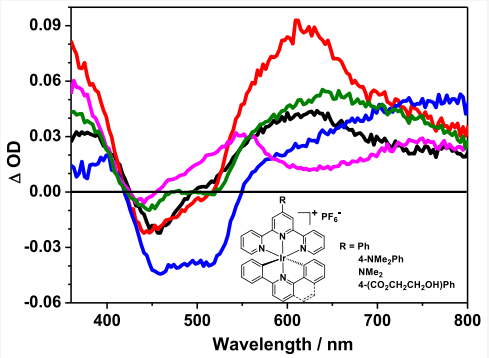

INTRODUCTION

In the past 20 years, octahedral d^6 iridium(III) complexes have gained intense interest because of their rich photophysical properties, such as long-lived triplet excited states, high phosphorescence quantum yields, excellent emission color tunability, and good chemical and thermal stability.[1−4] Various Ir(III) complexes have been explored for a wide range of applications, including luminescent bioimaging,[5−11] photodynamic therapy (PDT),[8−17] low-power upconversion,[18,19] organic light-emitting diodes (OLED),[20,21] light-emitting electrochemical cells (LEECs),[22,23] nonlinear optics,[24−27] etc. Efficient tuning of the photophysical properties of the Ir(III) complexes for specific applications can be realized via structural modifications of the coordinating/cyclometalating ligands,[26−28] while understanding the structure−property correlations holds the key for developing Ir(III) complexes with predetermined properties.

Among the various Ir(III) complexes, tris-bidentate Ir(III) complexes bearing cyclometalating ligands, such as Ir(C^N)$_3$ and (C^N)$_2$Ir(N^N)$^+$ (where C^N denotes the cyclometalating ligands and N^N represents the diimine ligands), are the most widely studied prototypes.[3,25,26] 2-Phenylpyridine (ppy) and its derivatives have been the most utilized cyclometalating ligands owing to their ease of synthesis and determinable photophysical properties for the resultant Ir(III) complexes. Optimization of the absorption and emission characteristics of these complexes can be realized through introducing electron-donating/-withdrawing substituents or fusing aromatic rings on the C^N and/or N^N ligands.[17,21−28]

In contrast to the tris-bidentate cyclometalated Ir(III) complexes, bis-terdentate Ir(III) complexes endow important advantages due to their axial symmetry that precludes geometrical isomers and facile tuning of intramolecular charge transfer.[29] However, most of the reported bis-terdentate Ir(III) complexes are the bis-terpyridine (tpy) complexes Ir-

Received: March 31, 2020
Published: June 4, 2020

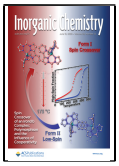

https://dx.doi.org/10.1021/acs.inorgchem.0c00961
Inorg. Chem. 2020, 59, 8532−8542

Scheme 1. Structures and Synthetic Route for (C^N^C)Ir(tpy)$^+$ Complexes Ir1−Ir5

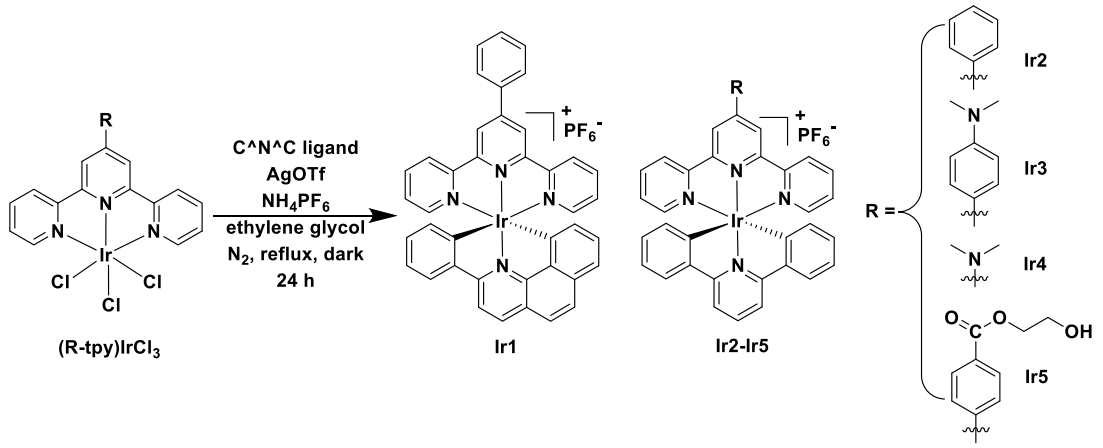

$(tpy)_2^{3+}$.[16,30−34] Studies on other types of bis-terdentate Ir(III) complexes, especially those with *trans*-bis-cyclometalating ligands, have been quite limited.[29,30,34−37] The challenges probably arise from the harsh reaction conditions in synthesizing these complexes, including high reaction temperature (>180 °C), restrictions to light and oxygen, and low product yield. The groundbreaking work on using 2,6-diphenylpyridine (dppy) derivatives as the *trans*-bis-cyclometalating ligand (C^N^C) was reported by Scandola and co-workers.[35,36] It was revealed that the heteroleptic linearly arranged (C^N^C)-Ir(tpy)$^+$ complexes exhibited bathochromically shifted charge transfer absorption and emission in comparison to their bis-terpyridine counterparts $Ir(tpy)_2^{3+}$.[35−37] These changes were rationalized by the stronger σ-donating ability of the C^N^C ligand, which raised the C^N^C- and metal-based highest occupied molecular orbital (HOMO) and the lowest singly occupied molecular orbital (*l*-SOMO), consequently lowering the ligand-to-ligand charge transfer (LLCT)/metal-to-ligand charge transfer (MLCT) absorption and emitting states.[35−37] The substituents (CH_3 or Br) on the 4′-phenyl group of the tpy ligand manifest some effects on the emission energies, while substitution on the 4-phenyl ring of the C^N^C ligand had a negligible effect on the emission energies of the complexes. Nonetheless, the types of substituents investigated have been quite limited, and exploration of the potential applications of this type of complexes is scarce.[35−37] To the extent of our knowledge, the only reported work on utilizing a (C^N^C)Ir(tpy)$^+$ type complex is the selective photooxidation of DNA purine base.[37]

Since 2013, our group has systematically investigated the reverse saturable absorption (RSA, a nonlinear absorption in which the stronger excited-state absorption over the ground-state absorption enhances the absorptivity of a material when the incident light fluence increases) of cyclometalated tris-bidentate Ir(III) complexes.[17,24−27,38−50] Our ultimate goal has been to develop reverse saturable absorbers with broadband absorption in the visible to the NIR regions for optical limiting applications.[51] It is known that the predominant parameter determining the RSA strength is the ratio of the excited-state absorption (ESA) cross section (σ_{ex}) with respect to that of the ground state (σ_0) at the defined wavelength; a broadband reverse saturable absorber is anticipated to possess a very weak ground-state absorption but much stronger ESA at 400−900 nm. Although many of our studied tris-bidentate Ir(III) complexes display very strong RSA at 532 nm, the lack of ground-state absorption at the longer visible to NIR regions and the insufficient ESA intensity in the NIR regions hamper their potential as broadband reverse saturable absorbers. To date, the RSA of bis-terdentate Ir(III) complexes has not been investigated. Because the broad and strong ESA in the red spectral regions in some of the reported $Ir(tpy)_2^{3+}$ and (C^N^C)Ir(tpy)$^+$ complexes[16,34−36] (in some cases extending to the NIR regions) and their red-shifted ground-state absorption via appropriate substitution on the terpyridine ligand[16] are desirable features for RSA, the bis-terdentate Ir(III) complexes could exhibit a strong RSA in the long visible spectral regions. Moreover, the stronger σ-donating ability of the C^N^C ligand could further bathochromically shift the charge-transfer ground-state absorption bands in the (C^N^C)Ir(tpy)$^+$ type of complexes with respect to their corresponding $Ir(tpy)_2^{3+}$ types,[37] which would further broaden the RSA spectral region.

To verify this prediction, we have designed and synthesized a series of (C^N^C)Ir(tpy)$^+$ complexes bearing the *trans*-cyclometalating ligand dppy (or its derivative) and tpy ligand with different substituents: i.e., [(2-phenylbenzo[*h*]quinoline)-Ir(4′-phenyl-tpy)]$^+$ (**Ir1**), [(2,6-diphenylpyridine)Ir(4′-phenyl-tpy)]$^+$ (**Ir2**), [(2,6-diphenylpyridine)Ir(4′-(4-dimethylaminophenyl)-tpy)]$^+$ (**Ir3**), [(2,6-diphenylpyridine)Ir(4′-dimethylamino-tpy)]$^+$ (**Ir4**), [(2,6-diphenylpyridine)Ir(4′-(4-$HOCH_2CH_2OOC$-phenyl)-tpy)]$^+$ (**Ir5**) (the structures are shown in Scheme 1). A series of spectroscopic techniques and theoretical simulations were utilized to systematically study their photophysical properties. Their ESAs and RSAs at 532 nm were manifested as well. In comparison to **Ir2**, **Ir1** containing a C^N^C ligand with a fused additional phenyl ring allows for demonstration of the effects of expansive π conjugation in the C^N^C ligand. **Ir3**−**Ir5** have either strongly electron donating or withdrawing substituents on the tpy ligand to tune the photophysical properties and RSAs of these complexes.

EXPERIMENTAL SECTION

Synthesis and Characterization. All solvents and reagents were obtained from VWR Scientific and used as received unless otherwise mentioned. Silica gels (230−400 mesh) and Al_2O_3 gels (activated, neutral, Brockmann I) for column chromatography were purchased from Sorbent Technology. The ligand 2,6-diphenylpyridine (dppy) was obtained from Alfa Aesar, while 2-phenylbenzo[*h*]quinoline was synthesized according to the literature procedure.[52] The N^N^N ligands 4′-phenyl-2,2′:6′,2″-terpyridine,[53] 4′-(4-dimethylaminophen-

https://dx.doi.org/10.1021/acs.inorgchem.0c00961
Inorg. Chem. 2020, 59, 8532−8542

yl)-2,2′:6′,2″-terpyridine,[54] 4′-dimethylamino-2,2′:6′,2″-terpyridine,[55] 4′-(4-COOH-phenyl)-2,2′:6′,2″-terpyridine,[56] (4′-phenyl-tpy)$IrCl_3$,[57] and (4′-(4-COOH-phenyl)-tpy)$IrCl_3$/(4′-(4-$HOCH_2CH_2OOC$-phenyl)-tpy)$IrCl_3$[58] were prepared according to the procedures reported in the literature. The synthesis and characterization of (4′-(4-dimethylaminophenyl)-tpy)$IrCl_3$, (4′-dimethylamino-tpy)$IrCl_3$, and **Ir1**−**Ir5** are reported below. ^{1}H NMR spectroscopy, electrospray ionization high-resolution mass spectrometry (ESI-MS), and elemental analysis were used to characterize the structures of **Ir1**−**Ir5**. The NMR spectra were collected on a Bruker-400 spectrometer. ESI-MS data were obtained on a Waters Synapt G2-Si mass spectrometer. Elemental analyses were carried out by NuMega Resonance Laboratories, Inc. (San Diego, CA).

General Synthetic Procedure for (4′-R-tpy)$IrCl_3$. The ligand 4′-R-tpy (0.1 mmol, R = phenyl, 4-dimethylaminophenyl, dimethylamino, 4-COOH-phenyl) and $IrCl_3{\cdot}3H_2O$ (0.1 mmol) were added to 10 mL of ethylene glycol. The suspension was purged with N_2 and heated to 160 °C for 15 min in dark. After the mixture was cooled to room temperature, the precipitate was collected, washed with water (2 × 10 mL) and ethanol (2 × 10 mL), and then dried under vacuum to yield the target complex, which was used for the following reaction step without further purification.

It should be noted that when 4′-(4-COOH-phenyl)-tpy reacted with $IrCl_3{\cdot}3H_2O$, the resultant complex was presumed to be a mixture of (4′-(4-COOH-phenyl)-tpy)$IrCl_3$ and its ester (4′-(4-$HOCH_2CH_2OOC$-phenyl)-tpy)$IrCl_3$ due to the possible reaction between the carboxyl group and ethylene glycol at a high reaction temperature, as reported previously in the literature.[58] However, because of the poor solubility of the complexes, they were not separated and were used directly for the following reaction step, in which the higher reaction temperature (196 °C) and longer reaction time (24 h) could convert the remaining COOH group into an ester group and thus the pure complex (4′-(4-$HOCH_2CH_2OOC$-phenyl)-tpy)Ir(dppy)PF_6 (**Ir5**) was separated.

(4′-(4-Dimethylaminophenyl)-tpy)$IrCl_3$. With 4′-(4-dimethylaminophenyl)-tpy (35.2 mg, 0.1 mmol) and $IrCl_3{\cdot}3H_2O$ (35.2 mg, 0.1 mmol) as the starting materials, a dark red powder was obtained as the product (41 mg, 63%). ^{1}H NMR (400 MHz, d_6-DMSO): δ 9.21 (dd, J = 5.6, 1.0 Hz, 2H), 8.97 (s, 2H), 8.89 (d, J = 8.1 Hz, 2H), 8.27 (td, J = 7.9, 1.5 Hz, 2H), 8.13 (d, J = 9.0 Hz, 2H), 7.97−7.89 (m, 2H), 6.93 (d, J = 9.1 Hz, 2H), 3.10 (s, 6H).

(4′-Dimethylamino-tpy)$IrCl_3$. With 4′-dimethylamino-tpy (27.6 mg, 0.1 mmol) and $IrCl_3{\cdot}3H_2O$ (35.2 mg, 0.1 mmol) as the starting materials, a dark red powder was obtained as the product (45 mg, 78%). ^{1}H NMR (400 MHz, d_6-DMSO): δ 9.19 (d, J = 5.7 Hz, 2H), 8.72 (d, J = 7.4 Hz, 2H), 8.21 (t, J = 7.1 Hz, 2H), 7.90 (s, 2H), 7.89−7.83 (m, 2H), 3.46 (s, 6H).

General Procedure for the Synthesis of Ir1−Ir5. (4′-R-tpy)$IrCl_3$ (0.2 mmol), the C^N^C ligand (0.2 mmol), and AgOTf (154 mg, 0.6 mmol) in ethylene glycol (10 mL) were heated to reflux under an N_2 atmosphere at 196 °C for 24 h in the dark. After the mixture was cooled to rt, NH_4PF_6 (163 mg, 1.0 mmol) was added to the mixture and then stirring was continued at rt for 2 h. The formed AgCl precipitate and other black byproducts were removed using a flash silica gel column with methanol as eluent. After removal of methanol, deionized water was added to precipitate the crude product. The pure product was isolated by silica gel chromatography with CH_2Cl_2/acetonitrile as eluent (from 1/0 to 50/1, v/v). The orange or orange-red band was collected and dried under vacuum to afford the target complex.

Ir1. With (4′-phenyl-tpy)$IrCl_3$ (121 mg, 0.2 mmol) and 2-phenylbenzo[*h*]quinoline (51 mg, 0.2 mmol) as the starting materials, an orange powder was obtained as the product (11 mg, 6%). ^{1}H NMR (400 MHz, $CDCl_3$): δ 8.89 (s, 2H), 8.65 (d, J = 7.9 Hz, 2H), 8.40 (d, J = 8.6 Hz, 1H), 8.18 (dd, J = 8.0, 3.5 Hz, 3H), 7.87 (dd, J = 14.0, 7.8 Hz, 4H), 7.77 (d, J = 8.8 Hz, 1H), 7.71 (t, J = 7.8 Hz, 2H), 7.57 (t, J = 7.5 Hz, 1H), 7.47 (t, J = 7.1 Hz, 3H), 7.17−7.11 (m, 1H), 7.04 (dd, J = 11.6, 5.7 Hz, 3H), 6.83 (t, J = 6.8 Hz, 1H), 6.52 (d, J = 6.4 Hz, 1H), 6.36 (d, J = 6.7 Hz, 1H). ESI-HRMS (m/z): calcd for $[C_{40}H_{26}IrN_4]^+$, 755.1789; found, 755.1782. Anal. Calcd for $C_{40}H_{26}F_6IrN_4P{\cdot}1.2CH_2Cl_2{\cdot}0.8CH_3CN$: C, 49.69; H, 3.00; N, 6.50. Found: 49.65; H, 3.24; N, 6.77.

Ir2. With (4′-phenyl-tpy)$IrCl_3$ (121 mg, 0.2 mmol) and 2,6-diphenylpyridine (46 mg, 0.2 mmol) as the starting materials, an orange powder was obtained as the product (10 mg, 6%). ^{1}H NMR (400 MHz, CD_3OD): δ 9.19 (s, 2H), 8.84 (d, J = 7.8 Hz, 2H), 8.28−8.22 (m, 2H), 8.09 (s, 3H), 8.04−7.97 (m, 2H), 7.87 (d, J = 7.3 Hz, 2H), 7.80 (d, J = 5.2 Hz, 2H), 7.75 (t, J = 7.5 Hz, 2H), 7.66 (t, J = 7.4 Hz, 1H), 7.32 (ddd, J = 7.3, 5.8, 1.3 Hz, 2H), 6.96 (td, J = 7.8, 1.2 Hz, 2H), 6.74 (td, J = 7.3, 1.1 Hz, 2H), 6.23 (d, J = 6.6 Hz, 2H). ESI-HRMS (m/z): calcd for $[C_{38}H_{26}IrN_4]^+$, 731.1789; found, 731.1795. Anal. Calcd for $C_{38}H_{26}F_6IrN_4P{\cdot}0.2CH_2Cl_2$: C, 51.39; H, 2.98; N, 6.28. Found: C, 51.05; H, 3.26; N, 6.25.

Ir3. With (4′-(4-dimethylaminophenyl)-tpy)$IrCl_3$ (130 mg, 0.2 mmol) and 2,6-diphenylpyridine (46 mg, 0.2 mmol) as the starting materials, a red powder was obtained as the product (18 mg, 10%). ^{1}H NMR (400 MHz, d_6-DMSO): δ 9.28 (s, 2H), 9.00 (d, J = 8.1 Hz, 2H), 8.26 (d, J = 9.1 Hz, 2H), 8.16 (d, J = 7.6 Hz, 2H), 8.08 (d, J = 7.1 Hz, 1H), 8.06−8.00 (m, 2H), 7.89 (d, J = 7.3 Hz, 2H), 7.67 (d, J = 5.7 Hz, 2H), 7.37−7.30 (m, 2H), 6.96 (d, J = 9.0 Hz, 2H), 6.90 (t, J = 7.5 Hz, 2H), 6.67 (t, J = 7.3 Hz, 2H), 6.17 (d, J = 6.2 Hz, 2H), 3.08 (s, 6H). ESI-HRMS (m/z): calcd for $[C_{40}H_{31}IrN_5]^+$, 774.2211; found, 774.2201. Anal. Calcd for $C_{40}H_{31}F_6IrN_5P{\cdot}1.5H_2O$: C, 50.79; H, 3.62; N, 7.40. Found: C, 50.78; H, 3.99; N, 7.24.

Ir4. With (4′-dimethylamino-tpy)$IrCl_3$ (115 mg, 0.2 mmol) and 2,6-diphenylpyridine (46 mg, 0.2 mmol) as the starting materials, a red powder was obtained as the product (6.7 mg, 4%). ^{1}H NMR (400 MHz, d_6-DMSO): δ 8.84 (d, J = 8.1 Hz, 2H), 8.26 (s, 2H), 8.16 (d, J = 7.8 Hz, 2H), 8.08−7.97 (m, 3H), 7.91 (d, J = 7.7 Hz, 2H), 7.60 (d, J = 5.9 Hz, 2H), 7.28 (t, J = 6.0 Hz, 2H), 6.92 (t, J = 6.9 Hz, 2H), 6.73 (t, J = 6.7 Hz, 2H), 6.28 (d, J = 6.5 Hz, 2H), 3.48 (s, 6H). ESI-HRMS (m/z): calcd for $[C_{34}H_{27}IrN_5]^+$, 698.1898; found, 698.1898. Anal. Calcd for $C_{34}H_{27}F_6IrN_5P{\cdot}2H_2O$: C, 46.47; H, 3.56; N, 7.79. Found: C, 46.23; H, 3.61; N, 7.62.

Ir5. With the mixed (4′-(4-COOH-phenyl)-tpy)$IrCl_3$/(4′-(4-$HOCH_2CH_2OOC$-phenyl)-tpy)$IrCl_3$ (139 mg, 0.2 mmol if it was pure (4′-(4-$HOCH_2CH_2OOC$-phenyl)-tpy)$IrCl_3$) and 2,6-diphenylpyridine (46 mg, 0.2 mmol) as the starting materials, an orange powder was obtained as the product (11 mg, 6%). ^{1}H NMR (400 MHz, d_6-DMSO): δ 9.49 (s, 2H), 9.09 (d, J = 6.9 Hz, 2H), 8.55 (d, J = 8.3 Hz, 2H), 8.33 (d, J = 8.8 Hz, 2H), 8.23 (d, J = 8.4 Hz, 2H), 8.13 (ddd, J = 16.5, 9.3, 3.0 Hz, 3H), 7.95 (d, J = 7.5 Hz, 2H), 7.77 (d, J = 4.9 Hz, 2H), 7.46−7.38 (m, 2H), 6.98−6.90 (m, 2H), 6.76−6.68 (m, 2H), 6.18 (d, J = 7.6 Hz, 2H), 5.05 (s, 1H), 4.44−4.37 (m, 2H), 3.83−3.76 (m, 2H). ESI-HRMS (m/z): calcd for $[C_{41}H_{30}IrN_4O_3]^+$, 819.1949; found, 819.1953. Anal. Calcd for $C_{41}H_{30}F_6IrN_4O_3P$: C, 51.09; H, 3.14; N, 5.81. Found: C, 51.46; H, 3.33; N, 6.12.

Photophysical Study. The solvents used for the photophysical studies were spectroscopic grade and were obtained from Alfa Aesar. A Varian Cary 50 spectrophotometer was used for UV−vis spectral measurements. The emission spectra were recorded on a HORIBA FluoroMax-4 fluorometer/phosphorometer. The emission quantum yields of **Ir1**−**Ir5** in deaerated solutions were determined by the relative actinometry method,[59] in which a deaerated acetonitrile solution of $[Ru(bpy)_3]Cl_2$ (Φ_{em} = 0.097 in, λ_{ex} = 436 nm)[60] was utilized as the reference for all complexes. The nanosecond transient difference absorption (TA) spectra and triplet lifetimes of **Ir1**−**Ir5** in degassed acetonitrile solutions were studied on an Edinburgh LP920 laser flash photolysis spectrometer using the third-harmonic output (355 nm) of a Nd:YAG laser (Quantel Brilliant, 4.1 ns, 1 Hz) as the excitation light. The triplet excited-state molar extinction coefficients at the TA band maxima were estimated using the singlet depletion method.[61] To determine the triplet excited-state quantum yields of **Ir1**−**Ir5**, the relative actinometry method[62] was applied and SiNc (ε_{590} = 70000 M^{-1} cm^{-1}, Φ_T = 0.20) in benzene was used as the standard.[63]

Nonlinear Transmission Measurements. The RSA strengths of **Ir1**−**Ir5** were evaluated by nonlinear transmission measurements using a Quantel Brilliant 4.1 ns laser (the repetition rate was set to 10 Hz) as the light source. The concentrations of the acetonitrile

https://dx.doi.org/10.1021/acs.inorgchem.0c00961
Inorg. Chem. 2020, 59, 8532−8542

solutions were adjusted to reach a linear transmission of 80% at 532 nm in the cuvette with a 2 mm path length. The experimental setup and details resembled those reported by our group previously.[64] With an f = 40 cm plano-convex lens, the beam radius was ∼96 μm at the focal point.

Computational Methodology. All complexes of this series were optimized at the singlet ground state at the level of density functional theory (DFT)[65] using the B3LYP functional.[66] Ir was treated with the LANL2DZ[67] basis set that includes the effective core potential. All other atoms were treated with the 6-31G* basis set.[68,69] Dichloromethane was used as the solvent within the conductor-like polarizable continuum model (CPCM)[70] reaction field method.

Linear response time-dependent density functional theory (TD-DFT)[71] was used to calculate the singlet excited-state energy and oscillation strength of the transitions. For calculations of the excited states, the same functional, basis sets, and CPCM solvation method were used as those used for the ground-state calculations. Absorption spectra were plotted using the Gaussian function with the line-broadening parameter of 0.10 eV, which produced an acceptable agreement to the thermal broadening of experimental absorption spectra.

To calculate the emission energies, the analytical gradient TDDFT method was applied to optimize the lowest triplet state,[72] with the same functional and basis sets as in the ground-state calculations. A qualitative description of excited states was presented using natural transition orbitals (NTOs),[73] which represent special distribution of the excited electron/hole wave function. The Gaussian16 software package was used for all calculations.[74] The VMD software packages[75] were used to visualize the NTOs with 0.02 isovalue.

RESULTS AND DISCUSSION

Electronic Absorption. The absorption spectra of **Ir1**−**Ir5** in CH_2Cl_2 and in other solvents (acetonitrile, THF, toluene) are presented in Figure 1 and in Figure S1 in the Supporting Information, respectively. The associated absorption parameters, i.e. band maxima and molar extinction coefficients, are given in Table 1. In the studied concentration range between 1 × 10^{-6} and 1 × 10^{-4} mol L^{-1}, the absorption of **Ir1**−**Ir5** followed Beer's law, indicating the absence of ground-state aggregation below the concentration of 1 × 10^{-4} mol L^{-1}. The absorption spectra of all complexes shared similar features, with strong absorption bands below 400 nm and broad, moderately strong bands between 400 and 600 nm. Considering the large molar extinction coefficients, the intense absorption bands below 400 nm can be attributed to ligand-localized spin-allowed $^1\pi,\pi^*$ transitions, while the moderate absorption bands at 400−600 nm are tentatively assigned to charge-transfer (^{1}CT) transitions mixed with $^1\pi,\pi^*$ characters.

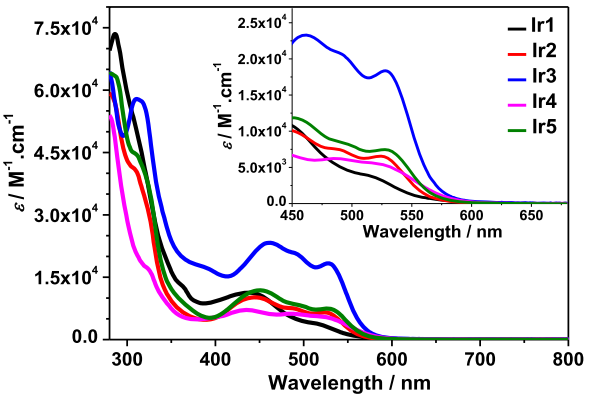

Figure 1. Experimental UV−vis absorption spectra of **Ir1**−**Ir5** at room temperature in CH_2Cl_2. The expanded spectra in the 450−650 nm regions are displayed as inset.

The assignment of the optical transitions making contributions to the absorption bands can be confirmed by the TDDFT calculations. As shown in Figure S2 in the Supporting Information, the calculated spectra matched well with the experimental spectra. The natural transition orbitals (NTOs) in Table 2 indicate that the lowest-energy absorption bands at 490−600 nm are dominated by the ligand-to-ligand charge transfer (^{1}LLCT)/metal-to-ligand charge transfer (^{1}MLCT) transitions in **Ir1**, **Ir2**, and **Ir5**, while the corresponding bands in **Ir3** and **Ir4** that bear the strongly electron donating dimethylaminophenyl or dimethylamino substituents have predominant R-tpy ligand localized ^{1}ILCT (intraligand charge transfer)/^{1}MLCT/$^1\pi,\pi^*$ characters. In contrast, the absorption bands at 400−490 nm in **Ir1**, **Ir2**, and **Ir5** are dominated by the R-tpy-based $^1\pi,\pi^*$/^{1}ILCT transitions admixing with some ^{1}MLCT/^{1}LLCT contributions, whereas these bands in **Ir3** and **Ir4** have predominant ^{1}LLCT/^{1}MLCT characters. For the absorption bands at <400 nm, the NTOs in Tables S1−S5 in the Supporting Information manifest the predominant $^1\pi,\pi^*$ nature, admixing with some charge transfer configurations.

Similar to those reported for (C^N^C)Ir(tpy)$^+$ complexes,[29,35−37] **Ir1**−**Ir5** exhibited greatly red-shifted and distinguishable ^{1}LLCT/^{1}MLCT absorption bands in the regions of 400−600 nm in comparison to that of the $Ir(tpy)_2^{3+}$ prototype[16,33] because of the stronger σ-donating capability of the *trans*-bis-cyclometalating C^N^C ligand. Fusing an additional phenyl ring in the C^N^C ligand in **Ir1** slightly increased the molar extinction coefficient of the $^1\pi,\pi^*$/^{1}LLCT/^{1}MLCT absorption band at 434 nm owing to the extended π conjugation of the C^N^C ligand in comparison to that in **Ir2**. However, the intensity of the lowest-energy absorption band at 517 nm in **Ir1** is the lowest among these five complexes. A careful examination of the NTOs corresponding to the S_1 transitions in these complexes (see Table 2) revealed that the S_1 transition in **Ir1** had the least contribution from the tpy-localized $^1\pi,\pi^*$ configuration, which accounted for the lower absorptivity of this absorption band in **Ir1** with respect to those in **Ir2**−**Ir4**. Considering the effect of the 4′-R substituents at the tpy ligand on the low-energy absorption bands, we can clearly see that the strongly electron donating 4-dimethylaminophenyl substituent drastically increased the molar extinction coefficients of these bands at 400−600 nm in **Ir3**; however, it did not change the transition energies of these bands. In contrast, the electron-withdrawing ester substituent evoked minor effects on either the energies or the molar extinction coefficients of the absorption bands in **Ir5** in comparison to those in **Ir2**. A comparison of the spectra of **Ir3** and **Ir4** found that the 4′-phenyl group at the tpy ligand played a distinct role in enhancing both the $^1\pi,\pi^*$ and ^{1}CT transitions associated with the tpy ligand but did not alter the transition energies.

Photoluminescence. The emission of **Ir1**−**Ir5** was investigated in CH_3CN, THF, CH_2Cl_2, and toluene + 5% CH_2Cl_2 at rt. The normalized emission spectra in CH_2Cl_2 are displayed in Figure 2, and the emission parameters are given in Table 1. The emission spectra and parameters in the other solvents are presented in Figure S3 and Table S6 in the Supporting Information. Upon excitation at the corresponding charge transfer bands, all complexes exhibited deep red emission, with the emission energies varying from 661 nm in **Ir1** to 688 nm in **Ir5** and the emission lifetimes falling into the

https://dx.doi.org/10.1021/acs.inorgchem.0c00961
Inorg. Chem. 2020, 59, 8532−8542

Table 1. Photophysical Properties of Complexes Ir1−Ir5

	λ_{abs}/nm (log ε)[a]	λ_{em}/nm (τ_{em}/μs); Φ_{em}[b]	k_r/s^{-1}[c]	k_{nr}/s^{-1}[d]	$\lambda_{T1\text{-}Tn}$/nm (τ_{TA}/μs; log ε_{T1-Tn}); Φ_T[e]
Ir1	286 (4.86), 434 (4.05), 517 (3.57)	661 (2.08); 0.072	5.17×10^4	6.66×10^5	375 (2.11; −), 625 (2.15; 4.34); 0.67
Ir2	280 (4.77), 308 (4.61), 445 (4.01), 527 (3.82)	678 (2.05); 0.033	2.06×10^4	6.05×10^5	360 (1.61; −), 612 (1.64; 4.64); 0.78
Ir3	280 (4.80), 311 (4.76), 461 (4.36), 528 (4.26)	679 (3.12); 0.049	3.27×10^4	6.35×10^5	399 (2.39; −), 768 (2.46; 4.52); 0.48
Ir4	280 (4.73), 324 (4.23), 437 (3.85), 528 (3.74)	676 (1.46); 0.015	6.04×10^4	3.97×10^6	366 (1.12; −), 550 (1.16; -), 750 (1.14; 4.54); 0.17
Ir5	283 (4.81), 309 (4.65), 450 (4.08), 529 (3.87)	688 (1.66); 0.022	5.30×10^4	2.36×10^6	360 (1.88; −), 639 (1.84; 4.88); 0.25

[a]Electronic absorption band maxima (λ_{abs}) and molar extinction coefficients (log ε) in CH_2Cl_2 at room temperature. [b]Room-temperature emission band maxima (λ_{em}) and lifetimes (τ_{em}) for **Ir1−Ir5** measured in CH_2Cl_2 ($c = 1 \times 10^{-5}$ mol L^{-1}). The emission quantum yields were obtained using $[Ru(bpy)_3]Cl_2$ ($\Phi_{em} = 0.097$, $\lambda_{ex} = 436$ nm) in a deaerated acetonitrile solution as the reference. [c]Radiative decay rates (k_r) calculated by $k_r = \Phi_{em}/(\Phi_T\tau_{em})$. [d]Nonradiative decay rates (k_{nr}) calculated by $k_{nr} = (1 - \Phi_{em})/(\Phi_T\tau_{em})$. [e]Nanosecond TA band maxima ($\lambda_{T1\text{-}Tn}$), triplet excited-state lifetimes (τ_{TA}), and quantum yield (Φ_T) measured in CH_3CN at room temperature.

Table 2. Natural Transition Orbitals (NTOs) for the Major Transitions Making Contributions to the Low-Energy Absorption Bands of Ir1−Ir5 in CH_2Cl_2

Excited state and properties	Hole	Electron	Excited state and properties	Hole	Electron
Ir1 S_1 525 nm $f = 0.004$	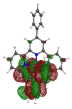	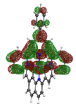	**Ir2** S_1 500 nm $f = 0.003$	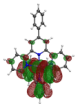	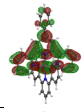
S_2 488 nm $f = 0.001$	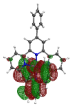	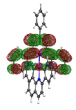	S_2 474 nm $f = 0.068$	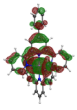	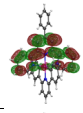
S_3 486 nm $f = 0.066$	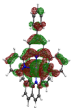	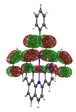	S_4 444 nm $f = 0.214$	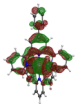	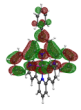
S_4 449 nm $f = 0.260$	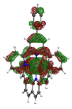	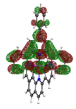	**Ir4** S_1 502 nm $f = 0.062$	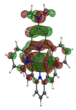	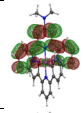
S_5 426 nm $f = 0.097$	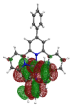	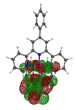	S_2 474 nm $f = 0.060$	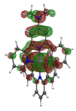	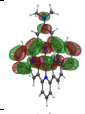
Ir3 S_1 529 nm $f = 0.022$	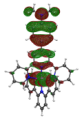	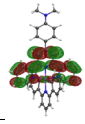	S_4 446 nm $f = 0.115$	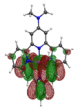	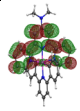
S_2 512 nm $f = 0.406$	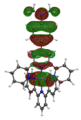	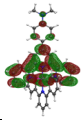	**Ir5** S_1 510 nm $f = 0.003$	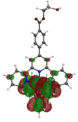	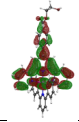
S_4 453 nm $f = 0.062$	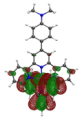	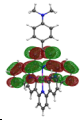	S_3 474 nm $f = 0.066$	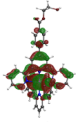	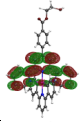
S_5 433 nm $f = 0.046$	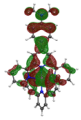	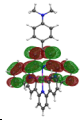	S_4 448 nm $f = 0.256$	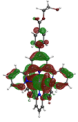	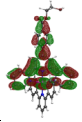

range of 1.46−3.12 μs in degassed CH_2Cl_2 solutions. The emission was subject to oxygen quenching, exhibited large red shifts in comparison to the excitation wavelengths, and possessed long-lived lifetimes. All of these features suggest a phosphorescent nature of the emission, which is in line with that reported for the other (C^N^C)Ir(tpy)$^+$ complexes in the literature.[29,35−37] In addition, the markedly red shifted but poorly resolved emission spectra are also in accordance with those observed for the other reported (C^N^C)Ir(tpy)$^+$ complexes,[29,35−37] while they are quite distinct from those reported for the $Ir(tpy)_2^{3+}$ complexes.[16,33,37]

The featureless emission bands and the 1.46−3.12 μs lifetimes of **Ir1−Ir5** imply a charge transfer character of the emitting state, which has been reported for the other

https://dx.doi.org/10.1021/acs.inorgchem.0c00961
Inorg. Chem. 2020, 59, 8532−8542

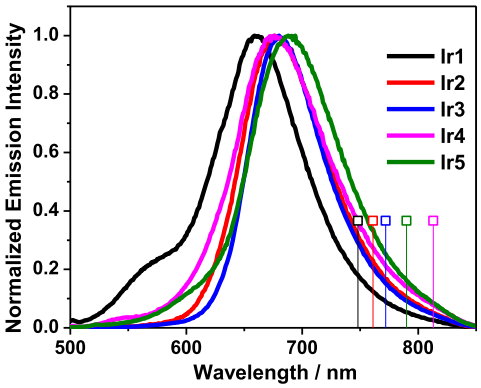

Figure 2. Normalized emission spectra of **Ir1** (λ_{ex} = 500 nm), **Ir2** (λ_{ex} = 460 nm), **Ir3** (λ_{ex} = 460 nm), **Ir4** (λ_{ex} = 460 nm), and **Ir5** (λ_{ex} = 450 nm) in the N_2-purged CH_2Cl_2 solution at room temperature (c = 1 × 10^{-5} mol L^{-1}). The sticks indicate the emission energies calculated by TDDFT using the B3LYP functional in CH_2Cl_2.

(C^N^C)Ir(tpy)$^+$ complexes in the literature.[29,35,36] However, in view of the very minor solvatochromic effects in different solvents with varied polarities (see Figure S3 in the Supporting Information), the emitting states should have significant ligand-centered $^3\pi,\pi^*$ configurations. This attribution is consistent with the recent report on the $(CH_3OPh\text{-}C^N^C)$-Ir$(HO_2CPh\text{-}tpy)^+$ complex.[37]

Further evidence supporting this assignment comes from the TDDFT calculation results via optimizing the lowest triplet excited states (T_1) of **Ir1**−**Ir5**. As shown in Table 3 and Figure 2, except for **Ir4**, the trend in the calculated emission energies for the other four complexes qualitatively matches the experimental emission energy trend. The off-trend of **Ir4** could arise from the underestimated lowest triplet-state energy that can be understood in terms of the ground-state triplet instability problem.[76] It has been reported that, in cases where the Hartree−Fock (HF) stability is less than ∼2 eV, the inclusion of exact HF exchange in the functional (e.g., 25% in B3LYP) leads to an artificial decrease in excitation energy of the triplet state. The lower degree of HF stability in **Ir4** in comparison to that in the other complexes is presumably rationalized by the lack of a phenyl ring in the substituent on the tpy ligand, which places the electron-donating $N(CH_3)_2$ group closer to the tpy ligand, resulting in a higher order of electron density redistribution between the substituent and the tpy ligand. However, this discrepancy in the excitation energy is expected to negligibly affect the special localization/delocalization properties of the excited wave function. The NTOs corresponding to the T_1 states of **Ir1**−**Ir5** illustrate that both the electrons and holes are predominantly distributed on the N^N^N ligands and the metal d orbitals, with the holes also containing slightly more distribution on the C^N^C ligand. Therefore, the nature of the emitting states in these complexes can be ascribed to the 4′-R-tpy ligand localized $^3\pi,\pi^*$ states admixing with some ^{3}MLCT/^{3}LLCT characters. For **Ir3**, the electron distribution of the holes is mainly on the 4′-(4-dimethylaminophenyl)pyridine motif and the metal d orbital, while the electron density is delocalized on the entire N^N^N ligand. Thus, the emitting state of **Ir3** has a significant ^{3}ILCT configuration in addition to the aforementioned $^3\pi,\pi^*$/^{3}MLCT/^{3}LLCT characters.

Table 3. NTOs Representing the Transitions That Contribute to the T_1 States of Ir1−Ir5 in CH_2Cl_2 Calculated by the TDDFT ΔSCF Method, Which Are Optimized with the B3LYP Functional and LANL2DZ/6-31G* Basis

	T_1 / nm	Hole	Electron
Ir1	748		
Ir2	761		
Ir3	772		
Ir4	813		
Ir5	790		

In comparison to the emission of **Ir2**, the emission energy of **Ir1** is increased, concomitant with a higher emission quantum yield but a similar emission lifetime. The increased emission quantum yield should be attributed to the much higher radiative decay rate (k_r) in **Ir1**. A closer examination of the holes of the T_1 states revealed an increased ^{3}LLCT character in the emitting state of **Ir1** in comparison to that of **Ir2** due to the π-extended C^N^C ligand in **Ir1**, which likely accounted for the increased k_r value and consequently a higher emission quantum yield in **Ir1** while the nonradiative decay rates remained similarly. Different from the effect of alteration of the cyclometalating ligand, incorporating a strongly electron donating dimethylamino substituent either on the 4′-phenyl ring or directly on the tpy ligand exerted a minor effect on the emission energies of **Ir3** and **Ir4**. However, these structural variations pronouncedly affected the emission lifetimes and quantum yields in **Ir3** and **Ir4** in comparison to those in **Ir2**. Complex **Ir3** with the dimethylamino substituent on the phenyl ring exhibited a longer emission lifetime and higher emission quantum yield, with the latter stemming from a 59% higher k_r value and a merely 5.0% higher k_{nr} value with respect to those of **Ir2**. In contrast, directly attaching the dimethylamino substituent to the tpy ligand in **Ir4** resulted in a 2.9-fold increase in k_r but a 6.6-fold increase in k_{nr} in comparison to those of **Ir2**, which shortened the emission lifetime and lowered the emission quantum yield for **Ir4**. On consideration of the effects of the electron-withdrawing ester group in **Ir5**, it caused a 10 nm bathochromic shift of the emission spectrum in comparison to that of **Ir2** due to the stabilization of the electron in the T_1 state by the electron-withdrawing substituent. Meanwhile, the k_r value was altered to 2.6-fold and k_{nr} to 3.9-fold increases with respect to those of **Ir2**. Consequently, the emission lifetime was shortened, and the quantum yield was reduced in **Ir5** in comparison to those in **Ir2**.

https://dx.doi.org/10.1021/acs.inorgchem.0c00961
Inorg. Chem. 2020, 59, 8532−8542

Transient Absorption (TA). TA spectroscopy is a powerful technique to provide further information on the triplet excited-state absorption and decay characteristics. To better understand the triplet excited-state properties, especially to figure out the spectral regions where the excited-state absorption is stronger than that of the ground state, the nanosecond TA of **Ir1**−**Ir5** was studied in acetonitrile solutions at room temperature. Figure 3 displays the TA

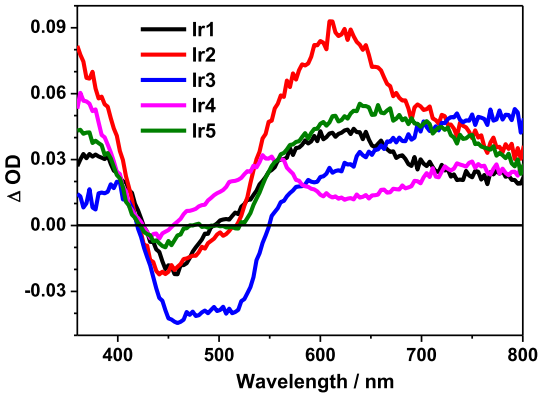

Figure 3. TA spectra of **Ir1**−**Ir5** in acetonitrile immediately after laser excitation (λ_{ex} = 355 nm). A_{355} = 0.4 in a 1 cm cuvette.

spectra immediately after 355 nm laser excitation, and the time-resolved TA spectra are provided in Figure S4 in the Supporting Information. The TA parameters such as the band maxima, triplet excited-state lifetimes deduced from the decay profiles of TA, and the T_1 state extinction coefficients and quantum yields are compiled in Table 1. The deduced TA lifetimes for **Ir1**−**Ir5** in acetonitrile are in line with their respective emission lifetimes in the same solution, indicating that the transient absorbing and emitting species originate from the same state. Considering the natures of the emitting states discussed in the section on emission, we can assign the observed TA signals from these complexes to the $^3\pi,\pi^*/^3$MLCT/^{3}LLCT T_1 states in these complexes, with the T_1 state in **Ir3** admixing with a significant ^{3}ILCT character.

As demonstrated in Figure 3, all complexes exhibited a positive TA band at 350−420 nm and broad and strong positive TA band(s) from the visible region extending to the NIR region (i.e., 496−800 nm for **Ir1**, 517−800 for **Ir2** and **Ir5**, 550−800 nm for **Ir3**, and 456−800 nm for **Ir4**). Bleaching occurred at the wavelengths essentially in accordance with the ^{1}CT bands in their respective UV−vis absorption spectra. The TA spectral features of **Ir1**, **Ir2**, and **Ir5** resembled each other; however, the TA signals were much stronger in **Ir2** with respect to those in **Ir1** and **Ir5**. This could be related to the highest triplet excited-state formation quantum yield of **Ir2** among these complexes. For **Ir3**, its broad TA band kept increasing in the NIR regions, which could be ascribed to the ^{3}ILCT character in its T_1 state. In contrast, the TA spectrum of **Ir4** was quite distinct from those of **Ir1**−**Ir3** and **Ir5** in that the positive TA bands were much broader with two band maxima at 550 and 750 nm, respectively. However, the TA intensities of **Ir4** were weaker in the entire TA spectrum in comparison to those of the other complexes. This reflects the absence of the phenyl ring in the N^N^N ligand in **Ir4**, confirming the involvement of the 4′-R-tpy ligand in the transient absorbing T_1 state in these complexes.

Reverse Saturable Absorption (RSA). We have manifested that many Ir(III) tris-bidentate complexes exhibited strong RSA and potentially could be utilized as optical limiting materials.[17,24−27,38−50] Generally, RSA requires a stronger excited-state absorption in comparison to the ground-state absorption at the same wavelength. The TA spectra in Figure 3 illustrated that all complexes, except for **Ir3**, hold positive signals at 532 nm, implying that the excited-state absorption at this wavelength was stronger than the ground-state absorption. This feature along with their much longer triplet excited-state lifetimes with respect to the pulse width of the laser beams (4.1 ns) indicate that RSA could occur at 532 nm from these complexes upon 532 nm nanosecond laser irradiation. To manifest this assumption, the nonlinear transmission measurements of **Ir1**−**Ir5** in a 2 mm cuvette in acetonitrile solutions were carried out using 4.1 ns laser pulses at 532 nm. The transmittance vs incident energy curves for **Ir1**−**Ir5** are presented in Figure 4. For comparison purposes, solutions with the same linear transmission of 80% at 532 nm in a 2 mm cuvette were employed.

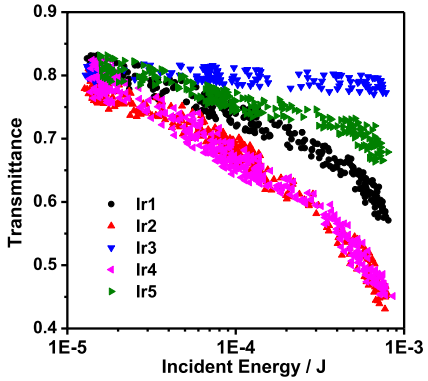

Figure 4. Nonlinear transmission plots of **Ir1**−**Ir5** in acetonitrile solutions with a linear transmittance of 80% in a 2 mm cuvette at 532 nm. The laser pulse duration was 4.1 ns.

Except for **Ir3**, the transmission of all the other complexes decreased with an increase in incident energy, suggesting that RSA took place. The strength of the RSA follows the trend **Ir2** ≈ **Ir4** > **Ir1** > **Ir5** > **Ir3**, which is essentially in accordance with their corresponding ΔOD values at 532 nm (i.e., 0.012 for **Ir1**, 0.024 for **Ir2**, −0.028 for **Ir3**, 0.026 for **Ir4**, and 0.008 for **Ir5**). The stronger RSAs of **Ir2** and **Ir4** are obviously related to their stronger excited-state absorption at 532 nm with respect to those of the other complexes, whereas the weaker excited-state absorption of **Ir3** in comparison to its ground-state absorption (as reflected by the negative ΔOD value) at 532 nm prevents the RSA in **Ir3**. However, in view of the much stronger TA signals at >585 nm for **Ir1**−**Ir3** and **Ir5**, the RSA of these complexes could be much stronger than that of **Ir4** at wavelengths longer than 585 nm. Nonetheless, **Ir4** holds the advantage of a broader excited-state absorption than the other complexes, making it a potential broadband reverse saturable absorber in the visible to the NIR spectral region.

CONCLUSIONS

Five bis-terdentate Ir(III) complexes bearing a *trans*-bis-cyclometalating ligand and a 4′-R-tpy ligand, i.e. (C^N^C)Ir-(R-tpy)$^+$, were synthesized to explore the effect of C^N^C ligand π conjugation and the 4′-R substituent at the tpy ligand

https://dx.doi.org/10.1021/acs.inorgchem.0c00961
Inorg. Chem. 2020, 59, 8532−8542

on the photophysics and excited-state absorption of these complexes to assess the feasibility of these types of complexes as reverse saturable absorbers. In comparison to the $Ir(tpy)_2^{3+}$ complexes, the stronger σ-donating ability of the C^N^C ligand caused a distinct red shift of the $^1CT/^1\pi,\pi^*$ bands to 400−600 nm. Although structural variations in either the cyclometalating or the tpy ligand exerted a minor effect on the energies of the $^1CT/^1\pi,\pi^*$ bands, these changes altered the molar extinction coefficients of these absorption bands drastically, especially that with the strongly electron donating 4′-(4-dimethylaminophenyl) substituent (**Ir3**). All complexes displayed deep red room-temperature phosphorescence (661−693 nm) in a variety of organic solvents (CH_2Cl_2, CH_3CN, THF, and toluene (with 5% CH_2Cl_2)) at room temperature. The emission spectrum of **Ir1** with a more π expansive C^N^C ligand was blue-shifted in all solvents in comparison to those of the other complexes bearing the 2,6-diphenylpyridine ligand, concomitant with the highest emission quantum yield. While introducing an electron-withdrawing ester substituent on the 4′-phenyl group of the tpy ligand caused a red shift of the emission spectrum for **Ir5** with a reduced emission quantum yield in comparison to those of **Ir2**, electron-donating 4′-(4-dimethylaminophenyl) and 4′-dimethylamino substituents on the tpy ligand had a minor effect on the emission energies of **Ir3** and **Ir4** with respect to that of **Ir2**. However, **Ir3** possessed a higher emission quantum yield with respect to that of **Ir2**, whereas the emission quantum yield was lower in **Ir4** in comparison to that of **Ir2**. All complexes exhibited broad and strong nanosecond TA bands in the visible to the NIR region originating from their $^3\pi,\pi^*/^3CT$ T_1 states. Structural alteration affected the spectral features and the TA signal intensities pronouncedly, with **Ir2** giving the strongest TA signals peaking at 612 nm, **Ir3** showing the highest TA signals in the NIR, and **Ir4** having the broadest TA bands at 456−800 nm. These complexes exhibited varying degrees of RSA at 532 nm, i.e. **Ir2** ≈ **Ir4** > **Ir1** > **Ir5** > **Ir3**, which primarily corresponded to their ΔOD values at 532 nm. In view of the strongest RSAs of **Ir2** and **Ir4** at 532 nm and their strong broadband TA signals, these two complexes hold the potential as broadband reverse saturable absorbers for optical limiting of nanosecond laser pulses.

■ ASSOCIATED CONTENT

Supporting Information

The Supporting Information is available free of charge at https://pubs.acs.org/doi/10.1021/acs.inorgchem.0c00961.

Normalized UV−vis absorption and emission spectra of **Ir1**−**Ir5** in different solvents, the time-resolved TA spectra of **Ir1**−**Ir5** in CH_3CN, comparison of the experimental and theoretical UV−vis absorption spectra of **Ir1**−**Ir5** in CH_2Cl_2, Cartesian coordinates of the optimized structures for **Ir1**−**Ir5** in CH_2Cl_2, NTOs for major transitions contributing to the absorption bands at <400 nm, the emission parameters of **Ir1**−**Ir5** in different solvents, and the full author list for refs 56 and 74. (PDF)

■ AUTHOR INFORMATION

Corresponding Author

Wenfang Sun − *Department of Chemistry and Biochemistry, North Dakota State University, Fargo, North Dakota 58108−6050, United States;* orcid.org/0000-0003-3608-611X; Phone: 701-231-6254; Email: Wenfang.Sun@ndsu.edu; Fax: 701-231-8831

Authors

Bingqing Liu − *Department of Chemistry and Biochemistry, North Dakota State University, Fargo, North Dakota 58108−6050, United States;* orcid.org/0000-0002-1540-2235

Mohammed A. Jabed − *Department of Chemistry and Biochemistry, North Dakota State University, Fargo, North Dakota 58108−6050, United States;* orcid.org/0000-0001-8552-0301

Svetlana Kilina − *Department of Chemistry and Biochemistry, North Dakota State University, Fargo, North Dakota 58108−6050, United States;* orcid.org/0000-0003-1350-2790

Complete contact information is available at: https://pubs.acs.org/10.1021/acs.inorgchem.0c00961

Notes

The authors declare no competing financial interest.

■ ACKNOWLEDGMENTS

The authors acknowledge the financial support of the National Science Foundation (NSF DMR-1411086 and CHE-1800476) for this work. S.K. also thanks the Center for Computationally Assisted Science and Technology (CCAST) at North Dakota State University for computational resources and administrative support.

■ REFERENCES

(1) Dixon, I. M.; Collin, J.-P.; Sauvage, J.-P.; Flamigni, L.; Encinas, S.; Barigelletti, F. A Family of Luminescent Coordination Compounds: Iridium(Iii) Polyimine Complexes. *Chem. Soc. Rev.* **2000**, *29*, 385−391.

(2) You, Y.; Park, S. Y. Phosphorescent Iridium(III) Complexes: Toward High Phosphorescence Quantum Efficiency through Ligand Control. *J. Chem. Soc. Dalt. Trans.* **2009**, *9226*, 1267−1282.

(3) You, Y.; Nam, W. Photofunctional Triplet Excited States of Cyclometalated Ir(III) Complexes: Beyond Electroluminescence. *Chem. Soc. Rev.* **2012**, *41*, 7061−7084.

(4) Zhao, J.; Wu, W.; Sun, J.; Guo, S. Triplet Photosensitizers: From Molecular Design to Applications. *Chem. Soc. Rev.* **2013**, *42*, 5323−5351.

(5) Chen, Y.; Rees, T. W.; Ji, L.; Chao, H. Mitochondrial Dynamics Tracking with Iridium(III) Complexes. *Curr. Opin. Chem. Biol.* **2018**, *43*, 51−57.

(6) You, Y. Phosphorescence Bioimaging Using Cyclometalated Ir(III) Complexes. *Curr. Opin. Chem. Biol.* **2013**, *17*, 699−707.

(7) Qiu, K.; Chen, Y.; Rees, T. W.; Ji, L.; Chao, H. Organelle-Targeting Metal Complexes: From Molecular Design to Bio-Applications. *Coord. Chem. Rev.* **2019**, *378*, 66−86.

(8) Ko, C.-N.; Li, G.; Leung, C.-H.; Ma, D.-L. Dual Function Luminescent Transition Metal Complexes for Cancer Theranostics: The Combination of Diagnosis and Therapy. *Coord. Chem. Rev.* **2019**, *381*, 79−103.

(9) Chen, Y.; Guan, R.; Zhang, C.; Huang, J.; Ji, L.; Chao, H. Two-Photon Luminescent Metal Complexes for Bioimaging and Cancer Phototherapy. *Coord. Chem. Rev.* **2016**, *310*, 16−40.

(10) Li, Y.; Tan, C. P.; Zhang, W.; He, L.; Ji, L. N.; Mao, Z. W. Phosphorescent Iridium(III)-Bis-N-Heterocyclic Carbene Complexes as Mitochondria-Targeted Theranostic and Photodynamic Anticancer Agents. *Biomaterials* **2015**, *39*, 95−104.

(11) He, L.; Li, Y.; Tan, C.-P.; Ye, R.-R.; Chen, M.-H.; Cao, J.-J.; Ji, L.-N.; Mao, Z.-W. Cyclometalated iridium(III) complexes as

lysosometargeted photodynamic anticancer and real-time tracking agents. *Chem. Sci.* **2015**, *6*, 5409−5418.
(12) Zamora, A.; Vigueras, G.; Rodríguez, V.; Santana, M. D.; Ruiz, J. Cyclometalated Iridium(III) Luminescent Complexes in Therapy and Phototherapy. *Coord. Chem. Rev.* **2018**, *360*, 34−76.
(13) Yang, Q.; Shi, M.; Zhao, H.; Lin, J.; An, L.; Cui, L.; Yang, H.; Zhou, Z.; Tian, Q.; Yang, S. Water-Soluble Polymer Nanoparticles Constructed by Three-Component Self-Assembly: An Efficient Theranostic Agent for Phosphorescent Imaging and Photodynamic Therapy. *Chem. Eur. J.* **2017**, *23*, 3728−3734.
(14) Majumdar, P.; Yuan, X.; Li, S.; Le Guennic, B.; Ma, J.; Zhang, C.; Jacquemin, D.; Zhao, J. Cyclometalated Ir(III) Complexes with Styryl-BODIPY Ligands Showing near IR Absorption/Emission: Preparation, Study of Photophysical Properties and Application as Photodynamic/Luminescence Imaging Materials. *J. Mater. Chem. B* **2014**, *2*, 2838−2854.
(15) Wang, L.; Monro, S.; Cui, P.; Yin, H.; Liu, B.; Cameron, C. G.; Xu, W.; Hetu, M.; Fuller, A.; Kilina, S.; McFarland, S. A.; Sun, W. Heteroleptic Ir(III)N_6 Complexes with Long-Lived Triplet Excited States and *In Vitro* Photobiological Activities. *ACS Appl. Mater. Interfaces* **2019**, *11*, 3629−3644.
(16) Liu, B.; Monro, S.; Li, Z.; Jabed, M. A.; Ramirez, D.; Cameron, C. G.; Colon, K.; Roque, J., III; Kilina, S.; Tian, J.; McFarland, S. A.; Sun, W. A New Class of Homoleptic and Heteroleptic Bis-(terpyridine) Iridium(III) Complexes with Strong Photodynamic Therapy Effects. *ACS Appl. Bio Mater.* **2019**, *2*, 2964−2977.
(17) Wang, C.; Lystrom, L.; Yin, H.; Hetu, M.; Kilina, S.; McFarland, S. A.; Sun, W. Increasing the Triplet Lifetime and Extending the Ground-State Absorption of Biscyclometalated Ir(III) Complexes for Reverse Saturable Absorption and Photodynamic Therapy Applications. *Dalton Trans.* **2016**, *45*, 16366−16378.
(18) Lu, Y.; Wang, J.; McGoldrick, N.; Cui, X.; Zhao, J.; Caverly, C.; Twamley, B.; Ó Máille, G. M.; Irwin, B.; Conway-Kenny, R.; Draper, S. M. Iridium(III) Complexes Bearing Pyrene-Functionalized 1,10-Phenanthroline Ligands as Highly Efficient Sensitizers for Triplet−Triplet Annihilation Upconversion. *Angew. Chem., Int. Ed.* **2016**, *55*, 14688−14692.
(19) Sun, J.; Wu, W.; Guo, H.; Zhao, J. Visible-Light Harvesting with Cyclometalated Iridium(III) Complexes Having Long-Lived ^{3}IL Excited States and Their Application in Triplet-Triplet-Annihilation Based Upconversion. *Eur. J. Inorg. Chem.* **2011**, *2011*, 3165−3173.
(20) Kuo, H.-H.; Hsu, L.-Y.; Tso, J.-Y.; Hung, W.-Y.; Liu, S.-H.; Chou, P.-T.; Wong, K.-T.; Zhu, Z.-L.; Lee, C.-S.; Jen, A. K.-Y.; et al. Blue-Emitting Bis-Tridentate Ir(III) Phosphors: OLED Performances *vs.* Substituent Effects. *J. Mater. Chem. C* **2018**, *6*, 10486−10496.
(21) Mróz, W.; Ragni, R.; Galeotti, F.; Mesto, E.; Botta, C.; De Cola, L.; Farinola, G. M.; Giovanella, U. Influence of Electronic and Steric Effects of Substituted Ligands Coordinated to Ir(III) Complexes on the Solution Processed OLED Properties. *J. Mater. Chem. C* **2015**, *3*, 7506−7512.
(22) Martínez-Alonso, M.; Cerdá, J.; Momblona, C.; Pertegás, A.; Junquera-Hernández, J. M.; Heras, A.; Rodríguez, A. M.; Espino, G.; Bolink, H.; Ortí, E. Highly Stable and Efficient Light-Emitting Electrochemical Cells Based on Cationic Iridium Complexes Bearing Arylazole Ancillary Ligands. *Inorg. Chem.* **2017**, *56*, 10298−10310.
(23) Zeng, Q.; Li, F.; Guo, T.; Shan, G.; Su, Z. Synthesis of Red-Emitting Cationic Ir(III) Complex and Its Application in White Light-Emitting Electrochemical Cells. *Org. Electron.* **2017**, *42*, 303−308.
(24) Li, Y.; Dandu, N.; Liu, R.; Hu, L.; Kilina, S.; Sun, W. Nonlinear Absorbing Cationic Iridium(III) Complexes Bearing Benzothiazolyl Fluorene Motif on the Bipyridine (N^N) Ligand: Synthesis, Photophysics and Reverse Saturable Absorption. *ACS Appl. Mater. Interfaces* **2013**, *5*, 6556−6570.
(25) Li, Z.; Cui, P.; Wang, C.; Kilina, S.; Sun, W. Nonlinear Absorbing Cationic Bipyridyl Iridium(III) Complexes Bearing Cyclometalating Ligands with Different Degrees of π-Conjugation: Synthesis, Photophysics, and Reverse Saturable Absorption. *J. Phys. Chem. C* **2014**, *118*, 28764−28775.
(26) Liu, B.; Lystrom, L.; Kilina, S.; Sun, W. Effects of Varying the Benzannulation Site and π Conjugation of the Cyclometalating Ligand on the Photophysics and Reverse Saturable Absorption of Monocationic Iridium(III) Complexes. *Inorg. Chem.* **2019**, *58*, 476−488.
(27) Liu, B.; Lystrom, L.; Brown, S. L.; Hobbie, E. K.; Kilina, S.; Sun, W. Impact of Benzannulation Site at the Diimine (N^N) Ligand on the Excited-State Properties and Reverse Saturable Absorption of Biscyclometalated Iridium(III) Complexes. *Inorg. Chem.* **2019**, *58*, 5483−5493.
(28) Li, T. Y.; Liang, X.; Zhou, L.; Wu, C.; Zhang, S.; Liu, X.; Lu, G. Z.; Xue, L. S.; Zheng, Y. X.; Zuo, J. L. N -Heterocyclic Carbenes: Versatile Second Cyclometalated Ligands for Neutral Iridium(III) Heteroleptic Complexes. *Inorg. Chem.* **2015**, *54*, 161−173.
(29) Jacques, A.; Auvray, T.; Bevernaegie, R.; Loiseau, F.; Cibian, M.; Hanan, G. S.; Mesmaeker, A. K.; Elias, B. Proton Sensitive Charge-Transfer Excited States in Bis-Terdentate Cyclometalated Ir(III) Complexes: Spectroscopic and Theoretical Investigation. *Inorg. Chim. Acta* **2018**, *471*, 8−16.
(30) Williams, J. A. G.; Wilkinson, A. J.; Whittle, V. L. Light-emitting Iridium Complexes with Tridentate Ligands. *Dalton Trans.* **2008**, 2081−2099.
(31) Lo, K. K.-W.; Chung, C.-K.; Nga, D. C.-M.; Zhu, N. Syntheses, Characterization and Photophysical Studies of Novel Biological Labelling Reagents Derived from Luminescent Iridium(III) Terpyridine Complexes. *New J. Chem.* **2002**, *26*, 81−88.
(32) Goldstein, D. C.; Cheng, Y. Y.; Schmidt, T. W.; Bhadbhade, M.; Thordarson, P. Photophysical Properties of A New Series of Water Soluble Iridium Bisterpyridine Complexes Functionalised at the 4′-Position. *Dalton Trans.* **2011**, *40*, 2053−2061.
(33) Collin, J.-P.; Dixon, I. M.; Sauvage, J.-P.; Williams, J. A. G.; Barigelletti, F.; Flamigni, L. Synthesis and Photophysical Properties of Iridium(III) Bisterpyridine and Its Homologues: a Family of Complexes with a Long-Lived Excited State. *J. Am. Chem. Soc.* **1999**, *121*, 5009−5016.
(34) Liu, B.; Monro, S.; Lystrom, L.; Cameron, C. G.; Colon, K.; Yin, H.; Kilina, S.; McFarland, S. A.; Sun, W. Photophysical and Photobiological Properties of Dinuclear Iridium(III) Bis-tridentate Complexes. *Inorg. Chem.* **2018**, *57*, 9859−9872.
(35) Polson, M.; Fracasso, S.; Bertolasi, V.; Ravaglia, M.; Scandola, F. Iridium Cyclometalated Complexes with Axial Symmetry. Synthesis and Photophysical Properties of a *trans*-Biscyclometalated Complex Containing the Terdentate Ligand 2,6-Diphenylpyridine. *Inorg. Chem.* **2004**, *43*, 1950−1956.
(36) Polson, M.; Ravaglia, M.; Fracasso, S.; Garavelli, M.; Scandola, F. Iridium Cyclometalated Complexes with Axial Symmetry. Time-Dependent Density Functional Theory Investigation of *trans*-Biscyclometalated Complexes Containing the Tridentate Ligand 2,6-Diphenylpyridine. *Inorg. Chem.* **2005**, *44*, 1282−1289.
(37) Jacques, A.; Mesmaeker, A. K.-D.; Elias, B. Selective DNA Purine Base Photooxidation by Bis-terdentate Iridium(III) Polypyridyl and Cyclometalated Complexes. *Inorg. Chem.* **2014**, *53*, 1507−1512.
(38) Liu, R.; Dandu, N.; Chen, J.; Li, Y.; Li, Z.; Liu, S.; Wang, C.; Kilina, S.; Kohler, B.; Sun, W. Influence of Different Diimine (N^N) Ligands on the Photophysics and Reverse Saturable Absorption of Heteroleptic Cationic Iridium(III) Complexes Bearing Cyclometalating 2-{3-[7-(Benzothiazol-2-yl)Fluoren-2-yl]Phenyl}pyridine (C^N) Ligands. *J. Phys. Chem. C* **2014**, *118*, 23233−23246.
(39) Li, Y.; Dandu, N.; Liu, R.; Li, Z.; Kilina, S.; Sun, W. Effects of Extended π-Conjugation in Phenanthroline (N^N) and Phenylpyridine (C^N) Ligands on the Photophysics and Reverse Saturable Absorption of Cationic Heteroleptic Iridium(III) Complexes. *J. Phys. Chem. C* **2014**, *118*, 6372−6384.
(40) Li, Y.; Dandu, N.; Liu, R.; Kilina, S.; Sun, W. Synthesis and Photophysics of Reverse Saturable Absorbing Heteroleptic Iridium-(III) Complexes Bearing 2-(7-R-Fluoren-2′-yl)Pyridine Ligands. *Dalt. Trans.* **2014**, *43*, 1724−1735.

https://dx.doi.org/10.1021/acs.inorgchem.0c00961
Inorg. Chem. 2020, 59, 8532−8542

(41) Pritchett, T. M.; Ferry, M. J.; Shensky, W. M.; Mott, A. G.; Stewart, D. J.; Long, S. L.; Haley, J. E.; Li, Z.; Sun, W. Strong Triplet Excited-State Absorption in a Phenanthrolinyl Iridium(III) Complex with Benzothiazolylfluorenyl-Substituted Ligands. *Opt. Lett.* **2015**, *40*, 186−189.
(42) Zhu, X.; Lystrom, L.; Kilina, S.; Sun, W. Tuning the Photophysics and Reverse Saturable Absorption of Heteroleptic Cationic Iridium(III) Complexes via Substituents on the 6,6′-Bis(fluoren-2-yl)-2,2′-biquinoline Ligand. *Inorg. Chem.* **2016**, *55*, 11908−11919.
(43) Liu, R.; Dandu, N.; McCleese, C.; Li, Y.; Lu, T.; Li, H.; Yost, D.; Wang, C.; Kilina, S.; Burda, C.; Sun, W. Influence of a Naphthaldiimide Substituent at the Diimine Ligand on the Photophysics and Reverse Saturable Absorption of Pt^{II} Diimine Complexes and Cationic Ir^{III} Complexes. *Eur. J. Inorg. Chem.* **2015**, *2015*, 5241−5253.
(44) Pei, C.; Cui, P.; McCleese, C.; Kilina, S.; Burda, C.; Sun, W. Heteroleptic Cationic Iridium(III) Complexes Bearing Naphthalimidyl Substituents: Synthesis, Photophysics and Reverse Saturable Absorption. *Dalton Trans.* **2015**, *44*, 2176−2190.
(45) Li, Z.; Li, H.; Gifford, B. J.; Peiris, W. D. N.; Kilina, S.; Sun, W. Synthesis, Photophysics, and Reverse Saturable Absorption of 7-(Benzothiazol-2-yl)-9,9-di(2-ethylhexyl)-9*H*-fluoren-2-yl Tethered $[Ir(bpy)(ppy)_2]PF_6$ and $Ir(ppy)_3$ Complexes (bpy = 2,2′-Bipyridine, ppy = 2-Phenylpyridine). *RSC Adv.* **2016**, *6*, 41214−41228.
(46) Sun, W.; Pei, C.; Lu, T.; Cui, P.; Li, Z.; McCleese, C.; Fang, Y.; Kilina, S.; Song, Y.; Burda, C. Reverse Saturable Absorbing Cationic Iridium(III) Complexes Bearing The 2-(2-Quinolinyl)quinoxaline Ligand: Effects of Different Cyclometalating Ligands on Linear and Nonlinear Absorption. *J. Mater. Chem. C* **2016**, *4*, 5059−5072.
(47) Zhu, X.; Cui, P.; Kilina, S.; Sun, W. Multifunctional Cationic Iridium(III) Complexes Bearing 2-Aryloxazolo[4,5-f][1,10]-Phenanthroline (N^N) Ligand: Synthesis, Crystal Structure, Photophysics, Mechanochromic/Vapochromic Effects, and Reverse Saturable Absorption. *Inorg. Chem.* **2017**, *56*, 13715−13731.
(48) Wang, L.; Cui, P.; Kilina, S.; Sun, W. Toward Broadband Reverse Saturable Absorption: Investigating the Impact of Cyclometalating Ligand π-Conjugation on the Photophysics and Reverse Saturable Absorption of Cationic Heteroleptic Iridium Complexes. *J. Phys. Chem. C* **2017**, *121*, 5719−5730.
(49) Wang, L.; Cui, P.; Kilina, S.; Sun, W. Heteroleptic Cationic Iridium(III) Complexes Bearing Phenanthroline Derivatives with Extended π-Conjugation as Potential Broadband Reverse Saturable Absorbers. *New J. Chem.* **2020**, *44*, 456−465.
(50) Liu, B.; Lystrom, L.; Cameron, C. G.; Kilina, S.; McFarland, S. A.; Sun, W. Monocationic Iridium(III) Complexes with Far-Red Charge-Transfer Absorption and Near-IR Emission: Synthesis, Photophysics, and Reverse Saturable Absorption. *Eur. J. Inorg. Chem.* **2019**, *2019*, 2208−2215.
(51) Zhou, G.-J.; Wong, W.-Y. Organometallic Acetylides of Pt^{II}, Au^{I} and Hg^{II} as New Generation Optical Power Limiting Materials. *Chem. Soc. Rev.* **2011**, *40*, 2541−2566.
(52) Li, A. H.; Beard, D. J.; Coate, H.; Honda, A.; Kadalbajoo, M.; Kleinberg, A.; Laufer, R.; Mulvihill, K. M.; Nigro, A.; Rastogi, P.; Sherman, D.; Siu, K.; Steinig, A.; Wang, T.; Werner, D.; Crew, A.; Mulvihill, M. One-Pot Friedländer Quinoline Synthesis: Scope and Limitations. *Synthesis* **2010**, *2010*, 1678−1686.
(53) Matias, T. A.; Mangoni, A. P.; Toma, S. H.; Rein, F. N.; Rocha, R. C.; Toma, H. E.; Araki, K. Catalytic Water-Oxidation Activity of a Weakly Coupled Binuclear Ruthenium Polypyridyl Complex. *Eur. J. Inorg. Chem.* **2016**, *2016*, 5547−5556.
(54) Bhowmik, S.; Ghosh, B. N.; Marjomäki, V.; Rissanen, K. Nanomolar Pyrophosphate Detection in Water and in a Self-Assembled Hydrogel of a Simple Terpyridine-Zn^{2+} Complex. *J. Am. Chem. Soc.* **2014**, *136*, 5543−5546.
(55) Ji, Z.; Azenkeng, A.; Hoffmann, M.; Sun, W. Synthesis and Photophysics of 4′-R-2,2′6′,2′-Terpyridyl (R = Cl, CN, $N(CH_3)_2$) Platinum(II) Phenylacetylide Complexes. *Dalt. Trans.* **2009**, *37*, 7725−7733.
(56) Martínez, M. Á.; Carranza, M. P.; Massaguer, A.; Santos, L.; Organero, J. A.; Aliende, C.; de Llorens, R.; Ng-Choi, I.; Feliu, L.; Planas, M.; et al. Synthesis and Biological Evaluation of Ru(II) and Pt(II) Complexes Bearing Carboxyl Groups as Potential Anticancer Targeted Drugs. *Inorg. Chem.* **2017**, *56*, 13679−13696.
(57) Chirdon, D. N.; Transue, W. J.; Kagalwala, H. N.; Kaur, A.; Maurer, A. B.; Pintauer, T.; Bernhard, S. $[Ir(N^N^N)(C^N)L]^+$: A New Family of Luminophores Combining Tunability and Enhanced Photostability. *Inorg. Chem.* **2014**, *53*, 1487−1499.
(58) Goldstein, D. C.; Cheng, Y. Y.; Schmidt, T. W.; Bhadbhade, M.; Thordarson, P. Photophysical Properties of a New Series of Water Soluble Iridium Bisterpyridine Complexes Functionalised at the 4′ Position. *Dalt. Trans.* **2011**, *40*, 2053−2061.
(59) Demas, J. N.; Crosby, G. A. The Measurement of Photoluminescence Quantum Yields. *J. Phys. Chem.* **1971**, *75*, 991−1024.
(60) Suzuki, K.; Kobayashi, A.; Kaneko, S.; Takehira, K.; Yoshihara, T.; Ishida, H.; Shiina, Y.; Oishi, S.; Tobita, S. Reevaluation of Absolute Luminescence Quantum Yields of Standard Solutions Using a Spectrometer with an Integrating Sphere and a Back-Thinned CCD Detector. *Phys. Chem. Chem. Phys.* **2009**, *11*, 9850−9860.
(61) Carmichael, I.; Hug, G. L. Triplet-Triplet Absorption Spectra of Organic Molecules in Condensed Phases. *J. Phys. Chem. Ref. Data* **1986**, *15*, 1−250.
(62) Kumar, C. V.; Qin, L.; Das, P. K. Aromatic Thioketone Triplets and Their Quenching Behaviour towards Oxygen and Di-t-Butylnitroxy Radical. A Laser-Flash-Photolysis Study. *J. Chem. Soc., Faraday Trans. 2* **1984**, *80*, 783−793.
(63) Firey, P. A.; Ford, W. E.; Sounik, J. R.; Kenney, M. E.; Rodgers, M. A. J. Silicon Naphthalocyanine Triplet State and Oxygen: A Reversible Energy-Transfer Reaction. *J. Am. Chem. Soc.* **1988**, *110*, 7626−7630.
(64) Guo, F.; Sun, W.; Liu, Y.; Schanze, K. Synthesis, Photophysics and Optical Limiting of Platinum(II) 4'-Tolylterpyridyl Arylacetylide Complexes. *Inorg. Chem.* **2005**, *44*, 4055−4065.
(65) Argaman, N.; Makov, G. Density Functional Theory: An Introduction. *Am. J. Phys.* **2000**, *68*, 69−79.
(66) Stephens, P. J.; Devlin, F. J.; Chabalowski, C. F.; Frisch, M. J. Ab Initio Calculation of Vibrational Absorption and Circular Dichroism Spectra Using Density Functional Force Fields. *J. Phys. Chem.* **1994**, *98*, 11623−11627.
(67) Roy, L. E.; Hay, P. J.; Martin, R. L. Revised Basis Sets for the LANL Effective Core Potentials. *J. Chem. Theory Comput.* **2008**, *4*, 1029−1031.
(68) Ditchfield, R.; Hehre, W. J.; Pople, J. A. Self-Consistent Molecular-Orbital Methods. IX. An Extended Gaussian-Type Basis for Molecular-Orbital Studies of Organic Molecules. *J. Chem. Phys.* **1971**, *54*, 724−728.
(69) Krishnan, R.; Binkley, J. S.; Seeger, R.; Pople, J. A. Self-Consistent Molecular Orbital Methods. XX. A Basis Set for Correlated Wave Functions. *J. Chem. Phys.* **1980**, *72*, 650−654.
(70) Barone, V.; Cossi, M.; Tomasi, J. Geometry Optimization of Molecular Structures in Solution by the Polarizable Continuum Model. *J. Comput. Chem.* **1998**, *19*, 404−417.
(71) Casida, M. E.; Jamorski, C.; Casida, K. C.; Salahub, D. R. Molecular Excitation Energies to High-Lying Bound States from Time-Dependent Density-Functional Response Theory: Characterization and Correction of the Time-Dependent Local Density Approximation Ionization Threshold. *J. Chem. Phys.* **1998**, *108*, 4439−4449.
(72) Furche, F.; Ahlrichs, R. Adiabatic Time-Dependent Density Functional Methods for Excited State Properties. *J. Chem. Phys.* **2002**, *117*, 7433−7447.
(73) Martin, R. L. Natural Transition Orbitals. *J. Chem. Phys.* **2003**, *118*, 4775−4777.
(74) Frisch, M. J.; Trucks, G. W.; Schlegel, H. B.; Scuseria, G. E.; Robb, M. A.; Cheeseman, J. R.; Scalmani, G.; Barone, V.; Petersson, G. A.; Nakatsuji, H., et al.. *Gaussian 16, Rev. B.01*; Gaussian, Inc.: Wallingford, CT, 2016.

https://dx.doi.org/10.1021/acs.inorgchem.0c00961
Inorg. Chem. 2020, 59, 8532−8542

(75) Humphrey, W.; Dalke, A.; Schulten, K. Sartorius Products. *J. Mol. Graphics* **1996**, *14*, 33−38.
(76) Peach, M. J. G.; Williamson, M. J.; Tozer, D. J. Influence of Triplet Instabilities in TDDFT. *J. Chem. Theory Comput.* **2011**, *7*, 3578−3585.

https://dx.doi.org/10.1021/acs.inorgchem.0c00961
Inorg. Chem. 2020, 59, 8532−8542